

The tilting rate of the Milky Way’s disc

Samuel W. F. Earp^{1*}, Victor P. Debattista¹, Andrea V. Macciò^{2,3},
David R. Cole⁴

¹ *Jeremiah Horrocks Institute, University of Central Lancashire, Preston, PR1 2HE, UK*

² *New York University Abu Dhabi, PO Box 129188, Saadiyat Island, Abu Dhabi, UAE*

³ *Max-Planck-Institute for Astronomy, Königstuhl 17, D-69117 Heidelberg, Germany*

⁴ *Rudolf Peierls Centre for Theoretical Physics, University of Oxford, Keble Road, Oxford, OX1 3NP, UK*

Accepted 2017 May 9. Received 2017 May 9; in original form 2016 October 13

ABSTRACT

We present tilting rates for galaxies comparable to the Milky Way (MW) in a Λ cold dark matter cosmological hydrodynamical simulation, and compare these with the predicted tilting rate detection limit of the *Gaia* satellite $0.28^\circ\text{Gyr}^{-1}$. We first identify galaxies with mass comparable to the MW ($9 \times 10^{11} \leq M_{200} \leq 1.2 \times 10^{12} M_\odot$) and consider the tilting rates between $z = 0.3$ and 0. This sample yields a tilting rate of $7.6^\circ \pm 4.5^\circ\text{Gyr}^{-1}$. We constrain our sample further to exclude any galaxies that have high stellar accretion during the same time. We still find significant tilting, with an average rate of 6.3°Gyr^{-1} . Both subsamples tilt with rates significantly above *Gaia*’s predicted detection limit. We show that our sample of galaxies covers a wide range of environments, including some similar to the MW’s. We find galaxies in denser regions tilt with higher rates than galaxies in less dense regions. We also find correlations between the angular misalignment of the hot gas corona, and the tilting rate. *Gaia* is likely to be able to directly measure tilting in the MW. Such a detection will provide an important constraint on the environment of the MW, including the rate of gas cooling onto the disc, the shape and orientation of its dark matter halo, and the mass of the Large Magellanic Cloud. Conversely, failure to detect tilting may suggest the MW is in a very quiet configuration.

Key words: Galaxy: disc – Galaxy: evolution – Galaxy: kinematics and dynamics – reference systems

1 INTRODUCTION

Disc galaxies such as the Milky Way (MW) are rapidly rotating; the orientation of their spin axis represents the integral of the angular momentum accreted via gas, interactions with satellites or other galaxies, and torques exerted on the disc by the dark matter halo within which they reside. Therefore directly observing disc tilting at the present time provides clues to the nature of each of these processes. The *Gaia* space astrometry mission may soon allow direct measurement of the MW’s disc tilting rate. Precision measurements will enable the construction of stellar position catalogues with accuracies of order 20μ as with respect to distant quasars, which act as the measurement reference frame (Perryman et al. 2001; Lindegren et al. 2008). Perryman et al. (2014) estimate that an accuracy better than $1\mu\text{as yr}^{-1}$ should be achieved in all the inertial spin

components of the *Gaia* reference frame, corresponding to $0.28^\circ\text{Gyr}^{-1}$.

Galaxies tilt for a variety of reasons. The role of interactions in disc tilting has been studied extensively. While major mergers destroy discs, smaller scale interactions are less violent, and tilt disc galaxies. Huang & Carlberg (1997) showed that infalling satellites tilt discs so that there is a preference for infalling satellites to merge in the plane of the disc. Read et al. (2008) reached a similar conclusion. Bett & Frenk (2012) investigated the effects of minor mergers and flybys on the orientation of spins of dark matter haloes of mass ($12.0 \leq \log_{10}(M/M_\odot) \leq 12.5$) at $z = 0$. They found that the majority of these events only caused small changes in the angular momentum of the entire halo, with only 10.5 per cent of MW mass haloes experiencing changes in their angular momentum by more than 45° over the course of their lifetimes. However, the inner halo is not so stationary, with 47 per cent of inner haloes experiencing a large change in their angular momentum orientation of

* E-mail: swfearp@gmail.com

at least 45° during their lifetimes. [Bett & Frenk \(2016\)](#) extended this study to include a broader range of halo masses ($10.5 \leq \log_{10}(M/M_\odot)h^{-1} \leq 15.5$). They found that 35 per cent of haloes had experienced changes in orientation of at least 45° , at some point in their lifetimes, without a major merger taking place.

In the MW, the most important ongoing interaction is with the Large and Small Magellanic Clouds (LMC and SMC). The mass of the LMC is currently the subject of debate, with mass estimates as high as $M_{\text{LMC}} \sim 2 \times 10^{11} M_\odot$ ([Kallivayalil et al. 2013](#); [Gómez et al. 2015](#); [Peñarrubia et al. 2016](#)), corresponding to ~ 20 per cent of the mass of the MW. Other estimates are significantly lower ($\sim 5 \times 10^9 M_\odot$) ([Alves & Nelson 2000](#); [van der Marel et al. 2002](#)). Thus the importance of the LMC on the orientation of the MW’s disc spin cannot yet be estimated well.

Another cause of disc tilting is torques from dark matter haloes. In the Λ -cold dark matter (Λ CDM) paradigm, haloes grow hierarchically, becoming triaxial ([Bardeen et al. 1986](#); [Barnes & Efstathiou 1987](#); [Frenk et al. 1988](#); [Dubinski & Carlberg 1991](#); [Jing & Suto 2002](#); [Bailin & Steinmetz 2005](#); [Allgood et al. 2006](#)). These triaxial haloes are themselves tilting ([Moore et al. 2004](#)). [Dubinski \(1992\)](#) examined the effect of tidal shear on dark matter haloes; he found that in all 14 of his $(1-2) \times 10^{12} M_\odot$ haloes the major axis rotated uniformly around the minor axis with a rotation rate in the range of $6^\circ-96^\circ \text{Gyr}^{-1}$. Likewise [Bailin & Steinmetz \(2004\)](#) measured figure rotation in 288 of their 317 dark matter haloes, finding a tilting rate of $6.2^\circ \text{Gyr}^{-1}$ with a log-normal distribution having $\sigma = 0.58^\circ \text{Gyr}^{-1}$. [Bryan & Cress \(2007\)](#) found that 63 per cent of the 115 haloes they considered exhibited significant figure rotation, with an average pattern speed of $13.8^\circ h \text{Gyr}^{-1}$.

The figure rotation of triaxial haloes leads to time varying torques on discs. [Debattista et al. \(2015\)](#) showed that a stellar disc, lacking gas, within a triaxial halo aligns its spin axis with the minor axis of the halo. Even when perturbed by a satellite the disc settles back to this alignment. Thus a tilting halo will drag a disc along with it. [Yurin & Springel \(2015\)](#) inserted live stellar discs into eight, MW-sized, high-resolution dark matter haloes from the AQUARIUS simulation. They found typical tilting rates of $5^\circ-6^\circ \text{Gyr}^{-1}$, comparable with halo tilting rates. While no direct evidence of tilting haloes exists, tidal torques exerted on a stellar disc by a rotating dark matter halo have been explored as a possible cause for warps ([Dubinski & Kuijken 1995](#); [Dubinski & Chakrabarty 2009](#)) and as a driving mechanism for spiral structure in dark matter-dominated galaxies ([Bureau et al. 1999](#)).

Galaxies such as the MW are generally thought to be surrounded by hot gas coronae, with masses greater than the stellar disc itself (e.g. [Spitzer 1956](#); [White & Rees 1978](#); [Savage & de Boer 1979](#); [White & Frenk 1991](#); [Dahlem 1997](#); [Wang et al. 2001](#); [Fukugita & Peebles 2006](#)). The quiescent cooling of this hot gas then sustains star formation over a long time ([Fall & Efstathiou 1980](#); [Brook et al. 2004](#); [Kereš et al. 2005](#); [Robertson et al. 2006](#); [Brooks et al. 2009](#)). However, the angular momentum of coronae is usually misaligned with that of their embedded stellar disc ([van den Bosch et al. 2002](#); [Roškar et al. 2010](#)). This contributes misaligned angular momentum to the disc, causing

its orientation to change. [Debattista et al. \(2015\)](#) showed that under these circumstances, the orientation of the disc spin is determined by a balance between the torques from the triaxial dark matter halo, and the net inflow of angular momentum via cooling gas. As a result, star forming galaxies are generally misaligned with the main planes of their dark matter haloes ([Sales & Lambas 2004](#); [Brainerd 2005](#); [Agustsson & Brainerd 2006](#); [Yang et al. 2006](#); [Azzaro et al. 2007](#); [Faltenbacher et al. 2007](#); [Wang et al. 2008, 2010](#); [Nierenberg et al. 2011](#); [Li et al. 2013](#)). [Debattista et al. \(2013\)](#) argued for just such an orientation in the MW, by noting that the best fitting models for the Sagittarius Stream ([Law et al. 2009](#); [Law & Majewski 2010](#); [Deg & Widrow 2013](#)) require the disc spin to be along the halo’s intermediate axis, an orientation they showed is extremely unstable. [Debattista et al. \(2013\)](#) therefore, argued that the modelling assumption of the disc residing in one of the symmetry planes must be violated. While this is indirect evidence, stacking of external galaxies has shown that the distribution of satellites around blue galaxies tends to be isotropic, contrary to what is seen around red galaxies ([Sales & Lambas 2004](#); [Brainerd 2005](#); [Yang et al. 2006](#); [Wang et al. 2008](#); [Nierenberg et al. 2011](#); [Wang et al. 2014](#); [Dong et al. 2014](#)).

In summary in the MW, the disc may be tilting for a variety of reasons. As a first step towards understanding the tilting of the MW, in this paper, we measure the tilting rates of MW-like galaxies in a Λ CDM cosmological simulation. We compare the tilting rates of these discs to the observational limit of *Gaia* to establish whether tilting of this nature would be detectable. In Section 2, we describe the cosmological simulation. Then in Section 3, we describe the samples of galaxies selected on the basis of virial mass, merger history and total satellite mass. In Section 4, we describe the methods we use to calculate the tilting rates. Section 5, presents the results, and provides a comparison with the observational limit of *Gaia* for a variety of different local configurations and environments. We present our conclusions in Section 6, showing that even galaxies in quiet systems tilt at a rate that would be detectable by *Gaia*.

2 NUMERICAL SIMULATION

The simulation we use here was performed with GASOLINE, a multi-stepping, parallel, tree code with smoothed particle hydrodynamics (SPH) ([Wadsley et al. 2004](#)). The version of GASOLINE used for this work includes radiative and Compton cooling for a primordial mixture of hydrogen and helium. The star formation algorithm is based on a Jeans instability criterion ([Katz 1992](#)), but simplified so that gas particles satisfying constant density, and temperature thresholds in convergent flows spawn star particles at a rate proportional to the local dynamical time (see [Stinson et al. 2006](#)). The star formation efficiency was set to 0.05 based on simulations of the MW that satisfied the Schmidt–Kennicutt Law ([Schmidt 1959](#); [Kennicutt 1998](#)), and we adopt a star formation threshold of 0.1 particles per cubic centimetre. The code also includes supernova feedback using the blast-wave formalism as described in [Stinson et al. \(2006\)](#), and a UV background following [Haardt & Madau \(1996\)](#); see [Governato et al. \(2007\)](#) for a more detailed description.

We used as a starting simulation one of the cosmological

cubes described in Macciò et al. (2008), namely our box has a size of 180Mpc and contained 300^3 dark matter particles. This box was created using WMAP5 (Komatsu et al. 2009) initial conditions with $(h, \Omega_M, \Omega_L, \Omega_b, \sigma_8) = (0.72, 0.258, 0.742, 0.0438, 0.796)$ and was run with the code PKDGRAV as detailed in Macciò et al. (2008).

From this simulation we selected at $z = 0$ a volume of about $(25 \text{ Mpc})^3$ with the requirement of not containing any haloes with a virial mass above $5 \times 10^{12} M_\odot$. For this purpose we use the halo catalogue from Macciò et al. (2008) which was generated using a Spherical Overdensity halo finder algorithm. The choice of this particular mass threshold is motivated by our interest in studying the properties of galaxies with a total mass equal or lower than the MW.

We then traced back to the initial conditions the Lagrangian region defined by this redshift-zero volume, making sure to obtain a continuous region (i.e. no holes) at the initial redshift ($z = 99$). Finally, we used the standard zoom-in technique to enhance the resolution of the dark matter particles in the selected region by a factor of 10^3 , and adding baryons (gas particles) with the same high resolution. As a final result, this high resolution region contains more than 10^8 particles, and reaches a mass resolution of 6.6×10^6 and $1.1 \times 10^6 M_\odot$ for dark matter and gas, respectively, with a gravitational softening length of 1.24 kpc for dark matter and 0.5 kpc for gas.

We then used the GASOLINE code described above to evolve these new high resolution initial conditions from $z = 99$ to 0 taking into account gas cooling, star formation and feedback in a self consistent way. To generate the catalogue of virially bound haloes we use the grid based code AMIGA Halo Finder (Knollmann & Knebe 2009) on the simulation outputs.

3 THE SAMPLES

We identify 182 haloes spanning the mass range $9 \times 10^{10} - 4.4 \times 10^{12} M_\odot$. Of the 41 saved time steps during the time interval $z = 0.3$ to 0 we use a subset of ten time steps with an average separation of $\sim 0.37 \text{ Gyr}$ to determine the stellar mass fractional growth rate, and to track the merger history of each galaxy. We calculate the tilting rate once for each galaxy, by measuring the angular momentum within 5 per cent of the virial radius at $z = 0.3$ and 0.

Subsample A contains haloes within a specified mass range comparable to the MW. The motivation for this mass cut is two-fold. First, we are interested in galaxies with similar halo mass as the MW. Secondly, we wish to choose galaxies where the mass of the dark matter halo, and the stellar mass are in good agreement with abundance matching results. We impose an upper limit of $M_{200} \leq 1.2 \times 10^{12} M_\odot$ in order to constrain the sample to a mass range that is comparable with the virial mass of the MW (Klypin et al. 2002). We also find that above this limit the full sample is dominated by ellipticals that, due to their evolutionary history, generally have lower specific angular momentum. Fig. 1 compares the halo mass–stellar mass relation of the full sample with the relation derived by the abundance matching method of Kravtsov et al. (2014). This figure shows that galaxies residing within haloes of mass $M_{200} \geq 9 \times 10^{11} M_\odot$ in the simulation match this relationship well. Lower mass

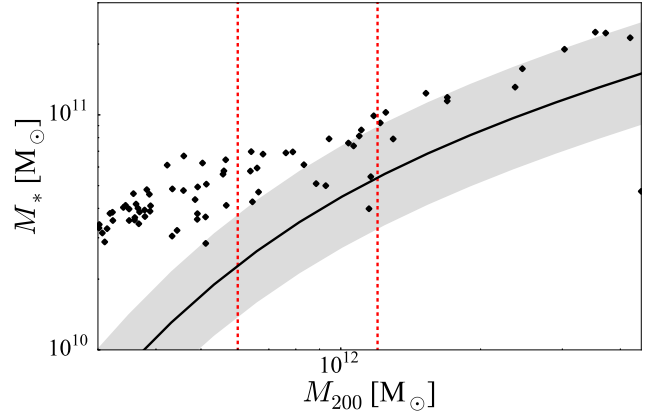


Figure 1. Stellar mass versus halo mass at redshift $z = 0$ for the most massive galaxies in the initial sample (black points). We measure the stellar mass within 5 per cent of the virial radius (r_{200}), where the mean interior density is 200 times the critical density. For comparison the black line shows the M_* – M_{200} relation of Kravtsov et al. (2014) derived using halo abundance matching. The grey shaded region shows the scatter in this relation. The red dashed lines illustrate the bounds that subsample A lies within.

haloes, however, have an excess stellar mass. Therefore, we use this mass as a lower limit for subsample A. Implementing the mass range $1.2 \times 10^{12} \geq M_{200} \geq 9 \times 10^{11} M_\odot$ leaves 19 galaxies in subsample A.

Subsample B has the same mass constraint with two added limits: one on the change in stellar mass to remove galaxies that have undergone mergers above a certain mass ratio, and the second on the ratio of galaxy mass to total satellite mass. First, we observe the evolution of the galaxies by visual inspection to construct a catalogue of galaxies that have not undergone mergers between $z = 0.3$ and 0. By comparing this catalogue to the full sample we can constrain the rate of change in stellar mass such that above this limit the sample is dominated by galaxies that have undergone mergers. Fig. 2 shows the distribution of fractional growth rates for galaxies that do not undergo mergers and the full sample. From Fig. 2 we set an upper limit on the maximum stellar mass fractional growth rate of 0.16 Gyr^{-1} within 5 per cent of the virial radius, under which galaxies have not undergone significant minor or major mergers. We construct subsample B from subsample A with the added constraint that $\Delta M_*/(\langle M_* \rangle \Delta t)$ must fall below this value. Two galaxies that fell below this limit were observed undergoing a minor merger, however, the maximum stellar mass accreted was roughly one per cent that of the central galaxy so they are included in subsample B. Lastly, we stipulate that the total satellite stellar mass must be less than 40 per cent that of the central galaxy at every time step. To measure the total satellite mass we subtract the total stellar mass within $0.1r_{200}$, where r_{200} is the virial radius, from the total stellar mass inside r_{200} . This leaves us with just seven galaxies in subsample B.

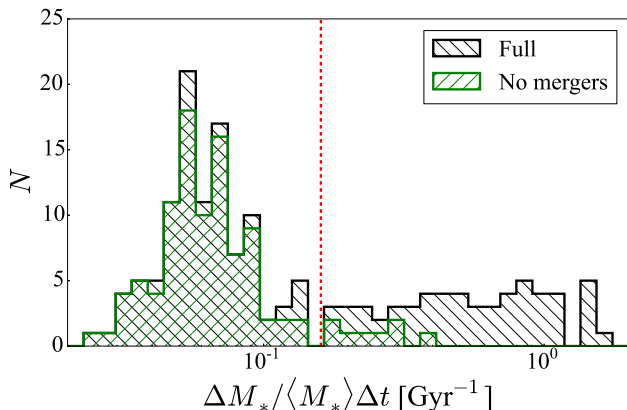


Figure 2. Distribution of the maximum rate of change in stellar mass normalized by average stellar mass between t_i and t_{i+1} within 5 per cent of the virial radius. The black histogram shows the rates for the full sample of 182 haloes. The green histogram shows the distribution of rates for galaxies that did not undergo any mergers between $z = 0.3$, and 0. The red dashed line indicates the upper limit we impose on subsample B.

4 ANALYSIS

To derive accurate tilting rates, we first find the kinematic centres of the galaxies. We adopt the position of the lowest potential dark matter particle as our kinematic centre. We verify that this method is reliable by computing the kinematic centre using an iterative shrinking sphere method. Starting with a sphere of 200 kpc, we iterate centring on the centre of mass and halving the radius each step to a final value of ~ 10 pc. Using the lowest potential dark matter particle, we are able to obtain kinematic centres for our entire sample of 182 galaxies.

We then measure the angular momentum of the galaxy by summing the angular momentum of each star particle within $R < 0.05r_{200}$. This radius is selected to include the disc of the galaxy, but exclude any warps. Briggs (1990) found that warps become detectable within the Holmberg radius (R_{Ho}). For a typical virial radius of ~ 200 kpc, we would expect a Holmberg radius of ~ 15 kpc, 5 kpc greater than the radius we would consider for $0.05r_{200} \sim 10$ kpc. We also select this radius to avoid selecting just the bulges of our galaxies, which tend to have lower specific angular momentum.

In order to determine the uncertainty in the tilting rates, we measure the difference in the direction of the angular momentum vector at different radii. We measure the angular momentum at seven linearly spaced radii spanning $0.01 < R/r_{200} < 0.04$. We then use the average angular discrepancy between the vectors as the error (σ) on the measurement of the angular momentum vector, and hence on the tilting rate. For each of these errors we assign a weight w such that $w = 1/\sigma^2$, which will be used in the calculation of the mean and standard deviation of each subsample.

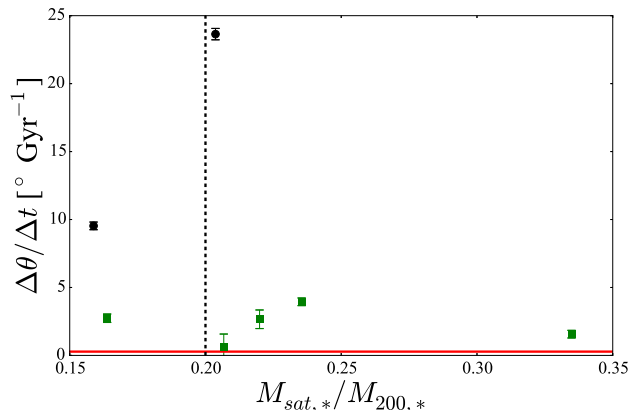


Figure 3. Tilting rate versus the present day fraction of satellite to galaxy stellar mass ($M_{\text{sat},*}/M_{200,*}$) for subsample B, i.e. galaxies that have mass comparable to the MW, and have low fractional stellar mass change between $z = 0.3$ and 0. The (green) squares represent the galaxies that were observed to not have undergone any mergers since $z = 0.3$, and 0. The (black) circles show the galaxies that undergo a minor merger. The black dashed line shows recent estimates of the mass ratio of the LMC relative to the MW (Kallivayalil et al. 2013; Gómez et al. 2015; Peñarrubia et al. 2016). The red horizontal line is *Gaia*'s predicted detection limit (Perryman et al. 2014).

5 RESULTS

5.1 Tilting rates

First we consider subsample A, i.e. galaxies with virial mass comparable to the MW's, within the range $9 \times 10^{11} \leq M_{200} \leq 1.2 \times 10^{12} M_{\odot}$. We measure the tilting rate once, between the two time steps $z = 0.3$ and 0. This subsample tilts with a mean rate of $7.6^{\circ}\text{Gyr}^{-1}$, and a standard deviation of $4.5^{\circ}\text{Gyr}^{-1}$, well above the average error for this subsample of just $0.05^{\circ}\text{Gyr}^{-1}$. All 19 of the galaxies in this subsample exhibit significant tilting above *Gaia*'s detection limit of $0.28^{\circ}\text{Gyr}^{-1}$ (Perryman et al. 2014).

Next we consider subsample B, i.e. the galaxies with similar mass to the MW, that have low fractional stellar mass change from $z = 0.3$ to $z = 0$, and have a maximum total satellite mass of 40 per cent that of the central galaxy. Fig. 3 shows tilting rates for sample B versus the ratio of stellar mass to satellite stellar mass. Each data point in this figure corresponds to a tilting rate of a single galaxy, with the mass ratio measured at $z = 0$. The green squares show only the five galaxies that were not observed to undergo any mergers since $z = 0.3$, while the black squares were the two galaxies that did undergo a minor merger within the same time. The tilting rates of this subsample have an average of $6.3^{\circ}\text{Gyr}^{-1}$, with a standard deviation of $6.5^{\circ}\text{Gyr}^{-1}$, well above the average uncertainty of $0.13^{\circ}\text{Gyr}^{-1}$. This subsample also tilts with a rate well above *Gaia*'s detection limit.

5.2 Environmental dependence

To determine if there is any dependence between the tilting rates of galaxies and their local environment, we compare the tilting rates of the galaxies with their normalized local density. We calculate the density within various radii centred

on each galaxy, and then normalize by the critical density at $z = 0$. Fig. 4 shows the distribution of densities for spheres with radii 3, 4, 5 and 6 Mpc. We find that for large radii (5 and 6 Mpc) that there is a strong correlation for subsample A with p values of 0.8 for both, although, for smaller radii (3 and 4 Mpc), the correlation weakens, with p values of 0.2 and 0.6 respectively. When we consider subsample B the correlations are enhanced, with p values of 0.7, 0.95, 0.97 and 0.96 for radii 3, 4, 5 and 6 Mpc, respectively.

The MW has a close massive neighbour M31 within 1 Mpc. We compare the tilting rates with the distance D to the nearest massive ($M_* > 9 \times 10^{11} M_\odot$) galaxy in subsample A. Fig. 5 shows the tilting rate versus D ; galaxies in subsample A span a range of D , including some with very close neighbours and some very isolated. We see no relation between D and the tilting rate. Considering galaxies in subsample B we do find a weak anti-correlation. One of our galaxies does appear to be tilting extremely fast without a close neighbour.

5.3 Dependence on gas

The angular momenta of the hot gas corona surrounding a galaxy and of the disc are not generally aligned. As the gas corona continually feeds cool gas to the disc, this misalignment causes gas being accreted to change the angular momentum of the disc. To investigate this effect on the tilting rate, we define the hot gas corona in two different ways. In the first, we choose all gas with a temperature $T > 5 \times 10^4 \text{K}$, and in the second, we choose all gas between two spherical shells of radii $0.2r_{200}$ and r_{200} . The angular momentum calculated from each definition is in good agreement, with $p = 0.99$. We compare the tilting rates of the hot gas corona to the tilting rate of the disc for both of these methods. Fig. 6 shows that for both methods of defining the corona, there is no correlation between the angular momentum tilting rate of the corona and disc for MW mass galaxies. Even when we consider subsample B, we find no correlation for both methods.

Next we compare the tilting rates of the disc to the angular misalignment between the disc and the hot gas corona for both methods of defining the hot gas corona. Figure 7 shows the relation between the tilting rates of discs and the angular misalignment of the hot gas corona and disc angular momentum. We find a weak correlation with p values of 0.4 and 0.5 for both methods, respectively, for subsample A. However, for subsample B, the correlation strengthens considerably for both methods with p values of 0.86 and 0.87.

The large-scale structure (LSS) may influence the flow of gas into the halo and subsequently the misalignment between the stellar and coronal angular momentum. When we compare the misalignment of the hot gas corona from the stellar disc with the normalized local density, we find similar correlations as those we found in Fig. 4. Therefore it is not possible to determine from this simulation if the effect of the environment directly governs the tilting of the galaxy, or if the LSS affects the tilting via its effect on the coronal angular momentum, as seems likely. [Debattista et al. \(2015\)](#) found that galaxies lacking gas generally aligned with the minor axis of their halo. However, when gas is allowed to cool on to the disc, the orientation can be more arbitrary. For both of our subsamples, we find that galaxies with higher

star formation generally tilt with higher rates. These results favour the gas driven tilting scenario.

When we compare the angular momentum misalignment between the disc and the gas corona with the local density, we find similar correlations as those in Fig. 4. Thus the mechanism by which the LSS affects the disc's tilting rate is unclear. The LSS may torque the disc directly, or it may influence the flow of gas into the halo, driving the misalignment between the stellar and coronal angular momentum, which in turn drives the tilting (e.g. [Debattista et al. 2015](#)). One possible clue comes from comparing the tilting and the star formation rate. For both of our subsamples, we find that galaxies with a higher star formation rate generally tilt faster, suggesting that it is the delivery of misaligned angular momentum through gas that dominates the tilting.

6 DISCUSSION AND CONCLUSIONS

When we consider galaxies with halo masses comparable to the MW (subsample A), we find significant tilting with an error weighted mean rate of $7.6^\circ \text{Gyr}^{-1}$ and a standard deviation of $4.5^\circ \text{Gyr}^{-1}$. The entire subsample displays significant tilting with rates higher than the detection limit of *Gaia*. We further restrict to a sample with low relative stellar accretion, and a maximum stellar mass fraction in satellites of 40 per cent (subsample B), finding a lower mean tilting rate of $6.2^\circ \text{Gyr}^{-1}$, with a range from 0.65 to $24.6^\circ \text{Gyr}^{-1}$.

A variety of processes may drive the change in angular momentum that we have measured. Interactions with other galaxies are the most violent processes changing the angular momentum of discs drastically over a short period. However, we have found that even when we exclude strong interactions we still measure significant tilting above the detection limit of *Gaia*. Therefore, we must turn to secular processes such as halo torques and the accretion of misaligned cold gas on to the disc to explain the entire phenomena of disc tilting.

We investigated the effect of the local environment on the tilting rate of the disc. Comparing the local density against the tilting rate, we find that the tilting rate does not correlate with the normalized local density within 3 Mpc for subsample A. However, for subsample B, we do find a correlation. When we consider larger radii, we find a correlation between the tilting rate and the local environment for both subsamples. Galaxies in denser regions generally tilt at higher rates than galaxies in lower density regions, irrespective of the galaxies stellar mass accretion.

The MW has a very close, similar mass, neighbour M31. In order to compare to the MW's configuration, we measured the distance to the nearest massive galaxy and determined the correlation with the tilting rates. We find almost no correlation for subsample A; however, for subsample B, we do find very weak anti-correlation. This suggests that the local configuration is unlikely to be a large contributing factor when the disc is accreting significant mass. Our sample contains galaxies in similar configurations to the MW with companion galaxies within a few hundred kpc; these galaxies exhibit tilting rates similar to more isolated galaxies.

To determine the effect of misaligned gas accreting from the hot gas corona, we measured both the tilting rate of the hot gas corona and the angular misalignment between the stars and the corona. We find no correlation between the

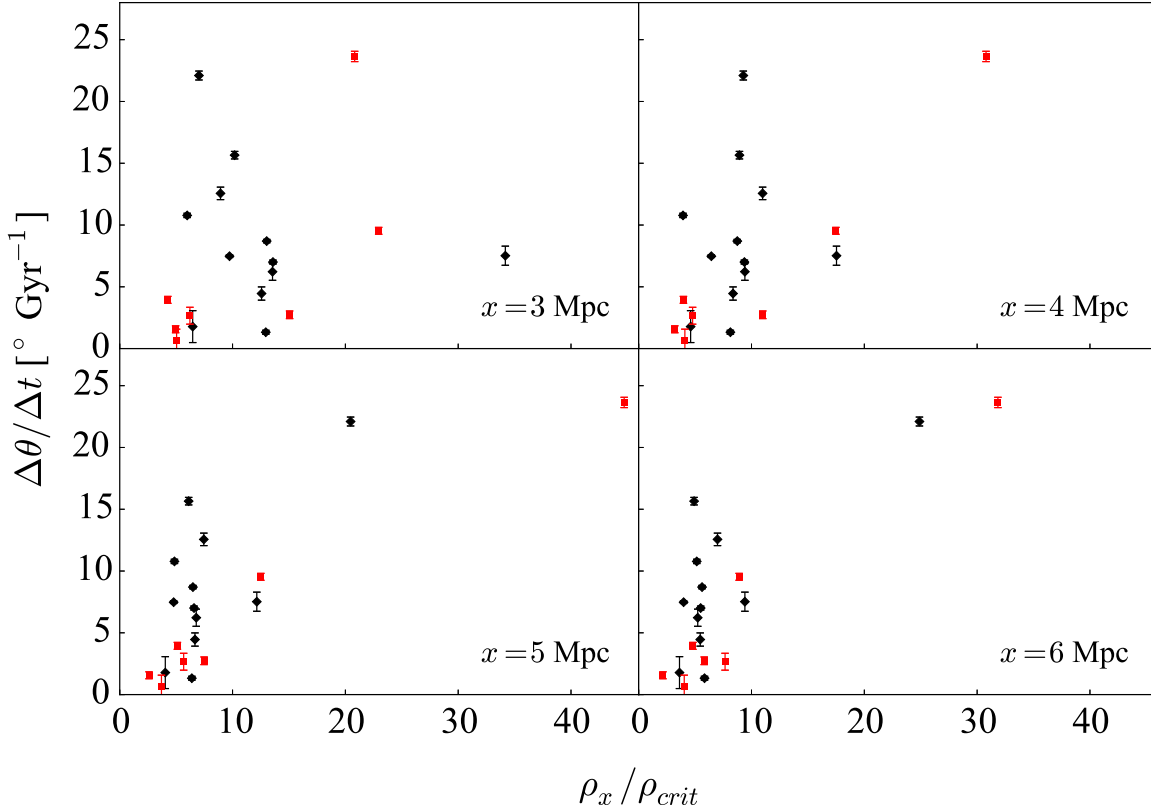


Figure 4. Tilting rate versus the local density within a sphere of radius x at redshift $z = 0$. In all panels, the (black) diamonds represent galaxies in subsample A with masses comparable to the MW, and the (red) squares show galaxies in subsample B with comparable mass and undergoing no interactions since $z = 0.3$. We measure correlation coefficients for each panel $x = 3, 4, 5$ and 6 Mpc of $p = 0.2, 0.6, 0.8$ and 0.8 , respectively, for all points, while for subsample B, we find p values of $0.7, 0.95, 0.98$ and 0.97 , respectively.

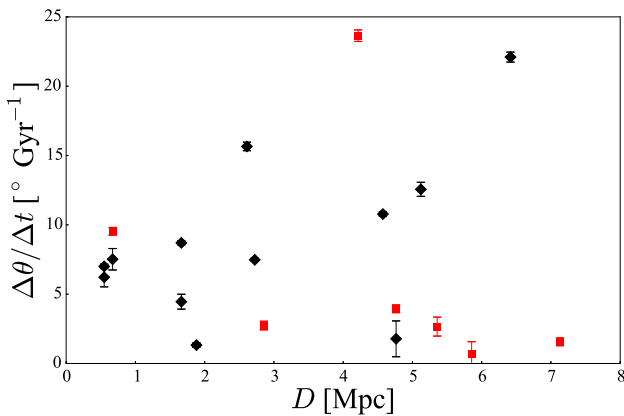


Figure 5. Tilting rate versus distance D to nearest galaxy with comparable mass to the MW measured at $z = 0$. The (black) diamonds represent subsample A and the (red) squares show subsample B. We find a correlation coefficient of $p = -0.05$ for subsample A and $p = -0.3$ for subsample B.

tilting rates of the two different components for either subsample. We also compared the tilting rate of the disc to the angular momentum misalignment between the two compo-

nents: For subsample A, there is a weak correlation, which becomes stronger for subsample B. We also find a correlation between the misalignment of the disc and coronal angular momentum and the LSS. Thus, the LSS may directly affect the tilting rate via torques, or indirectly by influencing the flow of gas into the halo. For both subsamples, galaxies with higher star formation tilt faster, perhaps indicating that the role of the LSS is in driving the misaligned gas. We conclude that the angular momentum misalignment between the corona and disc is an important, possibly dominant, driver of disc tilting.

In this paper, we have measured the tilting rates for a wide variety of galaxies of similar mass to the MW, in various configurations, some similar to the local configuration of the MW. Every configuration yielded a tilting rate above the *Gaia* limit and should be detectable. Confirmation of a tilting disc would have important consequences for understanding the evolution of the MW. For example, the tilt of the disc will make the potential seen by the Sagittarius Stream time varying. Conversely failure to detect tilting may suggest the MW is in an unexpectedly quiet configuration.

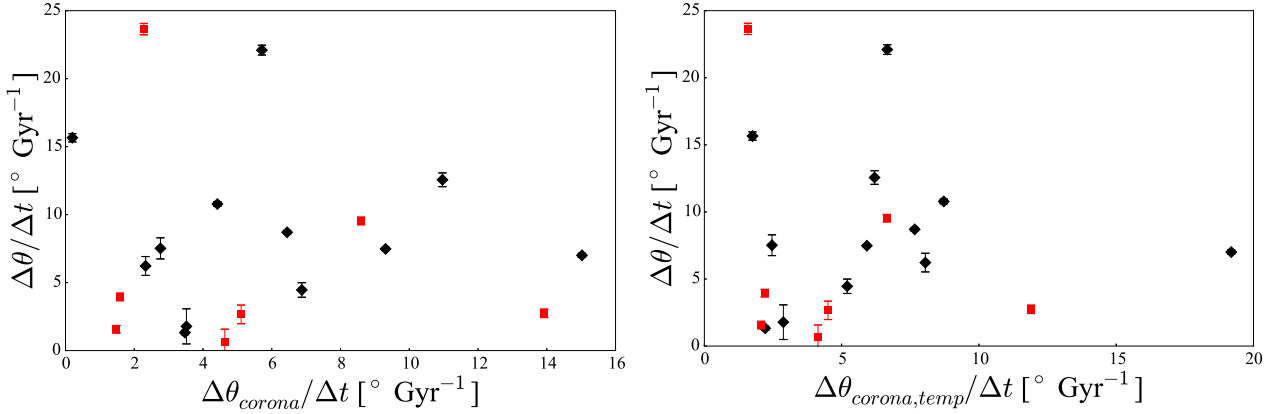


Figure 6. Left-hand panel: The tilting rate of the stellar disc versus the tilting rate of the corona, defined as all gas between radii $0.2r_{200}$ and r_{200} . We find no correlation for subsample A (black diamonds) with a coefficient of $p = -0.08$. For subsample B (red squares) we find no correlation with $p = -0.18$. Right-hand panel: The tilting rate of the stellar disc versus the tilting rate of the corona, defined as all gas with a temperature $T > 5 \times 10^4$ K. We find no significant correlation for subsample A (black diamonds), with $p = -0.035$. Similarly for subsample B (red squares) we find no correlation, with $p = -0.27$.

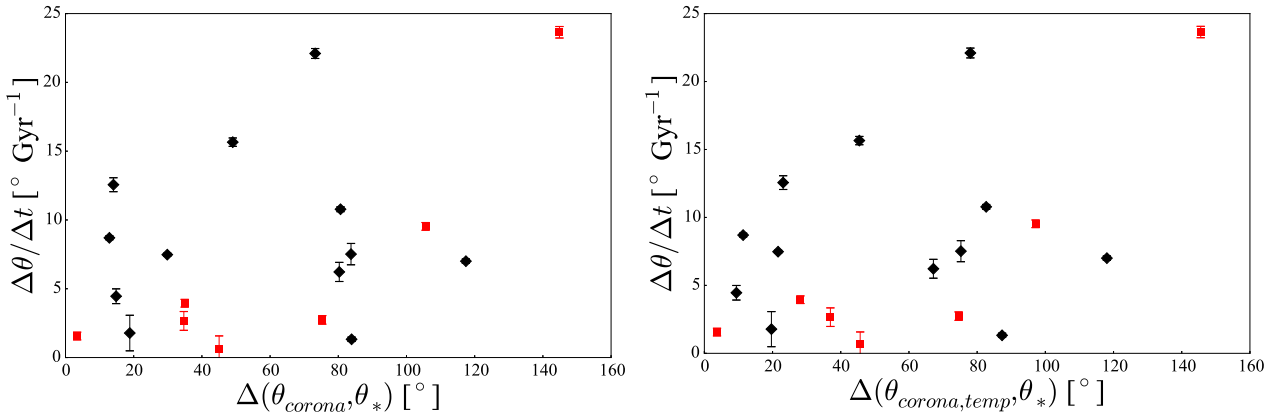


Figure 7. Left-hand panel: The tilting rate of the stellar disc versus the angular difference in angular momentum orientation between the stellar disc and the hot gas corona, defined as all gas between radii $0.2r_{200}$ and r_{200} . We find a weak correlation for subsample A (black diamonds), with $p = 0.4$, and a strong correlation for subsample B (red squares), with $p = 0.86$. Right-hand panel: The tilting rate of the stellar disc versus the difference in orientation between the stellar disc and the hot gas corona, defined as all gas with temperature $T > 5 \times 10^4$ K. We find a weak correlation for subsample A (black diamonds) with $p = 0.5$, and a strong correlation for subsample B (red squares) with $p = 0.87$.

ACKNOWLEDGEMENTS

SWFE would like to thank Dominic Bowman for useful conversations. VPD is supported by the Science and Technology Funding Council Consolidated grant #ST/M000877/1. VPD acknowledges the support of the Pauli Center for Theoretical Studies, which is supported by the Swiss National Science Foundation (SNF), the University of Zürich, and ETH Zürich. Simulations were performed at the Rechen Zentrum of the Max Planck Society in Garching (RZG) on the THEO and HYDRA machines.

REFERENCES

- Agustsson I., Brainerd T. G., 2006, *ApJ*, 650, 550
- Allgood B., Flores R. A., Primack J. R., Kravtsov A. V., Wechsler R. H., Faltenbacher A., Bullock J. S., 2006, *MNRAS*, 367, 1781
- Alves D. R., Nelson C. A., 2000, *ApJ*, 542, 789
- Azzaro M., Patiri S. G., Prada F., Zentner A. R., 2007, *MNRAS*, 376, L43
- Bailin J., Steinmetz M., 2004, *ApJ*, 616, 27
- Bailin J., Steinmetz M., 2005, *ApJ*, 627, 647
- Bardeen J. M., Bond J. R., Kaiser N., Szalay A. S., 1986, *ApJ*, 304, 15
- Barnes J., Efstathiou G., 1987, *ApJ*, 319, 575
- Bett P. E., Frenk C. S., 2012, *MNRAS*, 420, 3324
- Bett P. E., Frenk C. S., 2016, *MNRAS*, 461, 1338
- Brainerd T. G., 2005, *ApJ*, 628, L101
- Briggs F. H., 1990, *ApJ*, 352, 15
- Brook C. B., Kawata D., Gibson B. K., Freeman K. C., 2004, *ApJ*, 612, 894
- Brooks A. M., Governato F., Quinn T., Brook C. B., Wadsley J.,

- 2009, *ApJ*, 694, 396
- Bryan S. E., Cress C. M., 2007, *MNRAS*, 380, 657
- Bureau M., Freeman K. C., Pfizner D. W., Meurer G. R., 1999, *AJ*, 118, 2158
- Dahlem M., 1997, *PASP*, 109, 1298
- Debattista V. P., Roškar R., Valluri M., Quinn T., Moore B., Wadsley J., 2013, *MNRAS*, 434, 2971
- Debattista V. P., van den Bosch F. C., Roškar R., Quinn T., Moore B., Cole D. R., 2015, *MNRAS*, 452, 4094
- Deg N., Widrow L., 2013, *MNRAS*, 428, 912
- Dong X. C., Lin W. P., Kang X., Ocean Wang Y., Dutton A. A., Macciò A. V., 2014, *ApJ*, 791, L33
- Dubinski J., 1992, *ApJ*, 401, 441
- Dubinski J., Carlberg R. G., 1991, *ApJ*, 378, 496
- Dubinski J., Chakrabarty D., 2009, *ApJ*, 703, 2068
- Dubinski J., Kuijken K., 1995, *ApJ*, 442, 492
- Fall S. M., Efstathiou G., 1980, *MNRAS*, 193, 189
- Faltenbacher A., Li C., Mao S., van den Bosch F. C., Yang X., Jing Y. P., Pasquali A., Mo H. J., 2007, *ApJ*, 662, L71
- Frenk C. S., White S. D. M., Davis M., Efstathiou G., 1988, *ApJ*, 327, 507
- Fukugita M., Peebles P. J. E., 2006, *ApJ*, 639, 590
- Gómez F. A., Besla G., Carpintero D. D., Villalobos Á., O'Shea B. W., Bell E. F., 2015, *ApJ*, 802, 128
- Governato F., Willman B., Mayer L., Brooks A., Stinson G., Valenzuela O., Wadsley J., Quinn T., 2007, *MNRAS*, 374, 1479
- Haardt F., Madau P., 1996, *ApJ*, 461, 20
- Huang S., Carlberg R. G., 1997, *ApJ*, 480, 503
- Jing Y. P., Suto Y., 2002, *ApJ*, 574, 538
- Kallivayalil N., van der Marel R. P., Besla G., Anderson J., Alcock C., 2013, *ApJ*, 764, 161
- Katz N., 1992, *ApJ*, 391, 502
- Kennicutt Jr. R. C., 1998, *ApJ*, 498, 541
- Kereš D., Katz N., Weinberg D. H., Davé R., 2005, *MNRAS*, 363, 2
- Klypin A., Zhao H., Somerville R. S., 2002, *ApJ*, 573, 597
- Knollmann S. R., Knebe A., 2009, *ApJS*, 182, 608
- Komatsu E., et al., 2009, *ApJS*, 180, 330
- Kravtsov A., Vikhlinin A., Meshcheryakov A., 2014, preprint
- Law D. R., Majewski S. R., 2010, *ApJ*, 714, 229
- Law D. R., Majewski S. R., Johnston K. V., 2009, *ApJ*, 703, L67
- Li Z., Wang Y., Yang X., Chen X., Xie L., Wang X., 2013, *ApJ*, 768, 20
- Lindgren L., et al., 2008, in Jin W. J., Platais I., Perryman M. A. C., eds, IAU Symposium Vol. 248, IAU Symposium. pp 217–223, doi:10.1017/S1743921308019133
- Macciò A. V., Dutton A. A., van den Bosch F. C., 2008, *MNRAS*, 391, 1940
- Moore B., Kazantzidis S., Diemand J., Stadel J., 2004, *MNRAS*, 354, 522
- Nierenberg A. M., Auger M. W., Treu T., Marshall P. J., Fassnacht C. D., 2011, *ApJ*, 731, 44
- Peñarrubia J., Gómez F. A., Besla G., Erkal D., Ma Y.-Z., 2016, *MNRAS*, 456, L54
- Perryman M. A. C., et al., 2001, *A&A*, 369, 339
- Perryman M., Spergel D. N., Lindgren L., 2014, *ApJ*, 789, 166
- Read J. I., Lake G., Agertz O., Debattista V. P., 2008, *MNRAS*, 389, 1041
- Robertson B., Bullock J. S., Cox T. J., Di Matteo T., Hernquist L., Springel V., Yoshida N., 2006, *ApJ*, 645, 986
- Roškar R., Debattista V. P., Brooks A. M., Quinn T. R., Brook C. B., Governato F., Dalcanton J. J., Wadsley J., 2010, *MNRAS*, 408, 783
- Sales L., Lambas D. G., 2004, *MNRAS*, 348, 1236
- Savage B. D., de Boer K. S., 1979, *ApJ*, 230, L77
- Schmidt M., 1959, *ApJ*, 129, 243
- Spitzer Jr. L., 1956, *ApJ*, 124, 20
- Stinson G., Seth A., Katz N., Wadsley J., Governato F., Quinn T., 2006, *MNRAS*, 373, 1074
- Wadsley J. W., Stadel J., Quinn T., 2004, *New Astron.*, 9, 137
- Wang Q. D., Immler S., Walterbos R., Lauroesch J. T., Breitschwerdt D., 2001, *ApJ*, 555, L99
- Wang Y., Yang X., Mo H. J., Li C., van den Bosch F. C., Fan Z., Chen X., 2008, *MNRAS*, 385, 1511
- Wang Y., Park C., Hwang H. S., Chen X., 2010, *ApJ*, 718, 762
- Wang Y. O., Lin W. P., Kang X., Dutton A., Yu Y., Macciò A. V., 2014, *ApJ*, 786, 8
- White S. D. M., Frenk C. S., 1991, *ApJ*, 379, 52
- White S. D. M., Rees M. J., 1978, *MNRAS*, 183, 341
- Yang X., van den Bosch F. C., Mo H. J., Mao S., Kang X., Weinmann S. M., Guo Y., Jing Y. P., 2006, *MNRAS*, 369, 1293
- Yurin D., Springel V., 2015, *MNRAS*, 452, 2367
- van den Bosch F. C., Abel T., Croft R. A. C., Hernquist L., White S. D. M., 2002, *ApJ*, 576, 21
- van der Marel R. P., Alves D. R., Hardy E., Suntzeff N. B., 2002, *AJ*, 124, 2639

This paper has been typeset from a $\text{\TeX}/\text{\LaTeX}$ file prepared by the author.